XL CILAMCE
IBERO-LATIN AMERICAN CONGRESS ON COMPUTATIONAL METHODS IN ENGINEERING
NOVEMBER 11-14, 2019
Praiamar Natal Hotel & Convention
Natal, RN-BRAZIL

MLPG-MOM HYBRID MESHLESS METHOD APPLIED TO 2D UNBOUNDED SCATTERING PROBLEMS USING RPIM SHAPE FUNCTIONS

Amorim, Tiago V. L.[1]
Moreira, Fernando J. S.[2]
tiagovla@ufmg.br
fernandomoreira@ufmg.br
[1]*Graduate Program in Electrical Engineering, Federal University of Minas Gerais*
[2]*Department of Electronics Engineering, Federal University of Minas Gerais*
Pres. Antônio Carlos Avenue 6627, 31270-901, Minas Gerais / Belo Horizonte, Brazil
Resende, Úrsula C.[3]
resendeursula@des.cefetmg.br
[3]*Department of Electrical Engineering, Federal Center for Technological Education of Minas Gerais*
Amazonas Avenue 5253, 30421-169, Minas Gerais / Belo Horizonte, Brazil

Abstract. Meshless methods have increasingly gained attention in recent years. Nonetheless, similar to the Finite Element Method (FEM), they cannot properly handle unbounded domains. For scattering problems, however, the Method of Moments (MoM) is fairly well consolidated, efficient, and easily applied to unbounded homogeneous mediums. This work couples the MoM used to model the unbounded free space, with the traditional Meshless Local Petrov-Galerkin modeling of a dielectric bounded object. In the inner region, the meshless method uses shape functions generated by radial point interpolation with polynomial reproduction, whereas in the outer region, the MoM uses triangular shape functions to describe the surface currents. As both shape functions possess the delta Kronecker property, the coupling is straightforwardly imposed by forcing the continuity of the tangential components of the electromagnetic field. In order to evaluate the convergence of the method, the TEz and TMz plane wave scattering from a homogeneous dielectric circular cylinder was analyzed since it has a modal analytical solution, providing means to study the precision of the numerical results. Nevertheless, the formulation is applicable to any arbitrary cylindrical contour shape. Also knowing that meshless methods are quite flexible to handle material inhomogeneity, a 2-dimensional Lüneburg lens, which has a continuous permittivity profile, was analyzed, and its results were compared to FEM solutions. For both TMz and TEz polarizations, it was observed that the convergence rate remains nearly the same for the electromagnetic field and equivalent current densities. This technique also provided a good agreement for the near and far electromagnetic field calculation.

Keywords: Meshless Method, Method of Moments, Electromagnetic Scattering.

1 Introduction

In recent years, a set of so-called meshless methods have gained significant popularity. Amongst these are the smoothed particle hydrodynamics method (SPH) [1], the element free Galerkin method (EFG) [2] and the meshless local Petrov-Galerkin method (MLPG) [3]. A significant asset of these approaches, as their name implies, is that they do not require a structured distribution of nodes to construct the numerical formulation. Therefore, adding and subtracting nodes is easily accomplished in order to minimize the error in different regions. Mesh-free methods also achieve geometry flexibility, which may suggest their use on a broad range of scientific and engineering problems.

When it comes to unbounded domains, as the electromagnetic scattering problems, the solution can only be obtained through the truncation of the numerical domain at some distance sufficiently far from the scattering object. As seen developed by Resende et al. [4] using EFG, and Nicomendes et al. [5] using MLPG.

According to Gibson [6], the method of moments (MoM) is relatively well consolidated, efficient, and easily applied to unbounded homogeneous mediums. This led Resende et al. [7] to develop a coupled EFG/MoM method, which allows the use of the MoM to model the far field of an unbounded domain, while the EFG method is used in the near field. To achieve the result, both regions are coupled by forcing the continuity of the tangential components of the electromagnetic field at the interface.

This work proposes a new MLPG-MoM formulation that can be applied to any arbitrary cylindrical contour shape. In this case, the MoM, using triangular shape functions, is used to handle the unbounded free space, while the traditional MLPG, using radial point interpolation method (RPIM) with polynomial reproduction shape functions, models a dielectric bounded object. As both shape functions possess the delta Kronecker property, the coupling is straightforwardly imposed.

2 Mathematical Formulation

In this paper, an electromagnetic scattering problem is solved assuming that no parameter depends on the z-direction. A 2-dimensional analysis (on the x-y plane) is proposed for the scattering of an arbitrary cylindrical dielectric object. The hybrid formulation proposed here divides the space into 2 regions, which are dealt with different numerical methods. In this case, the inner region is limited by the object boundary and the outer region is the free space. The fields are assumed to be time-harmonic (with $e^{j\omega t}$ variation) in a source-free space.

2.1 Intern Region: Meshless Method

Assuming there is no variation in the z-direction ($\partial/\partial z = 0$), according to Peterson et al. [8], the characteristic equation to be dealt with is the inhomogeneous Helmholtz equation:

$$\nabla . \left(\frac{1}{p(\mathbf{x})} \nabla u^h(\mathbf{x}) \right) + k_0^2 q(\mathbf{x}) u^h(\mathbf{x}) = 0. \tag{1}$$

For the TMz polarization, u^h is the z-component of the electric field E_z, p is the relative magnetic permeability μ_r, and q is the relative electric permittivity ϵ_r. For the TEz polarization, u^h is the z-component of the magnetic field H_z, p is the relative electric permittivity ϵ_r, and q is the relative magnetic permeability μ_r. In both of the cases, k_0 is the free-space wavenumber ($k_0 = 2\pi/\lambda_0$, where λ_0 is the free-space wavelength).

Let Ω be the dielectric object material domain whose properties $p(\mathbf{x})$ and $q(\mathbf{x})$ are continuous functions of the position $\mathbf{x}$, and the boundary Γ. Applying the weighted residual method and the divergence theorem to Eq. (1), as described by Jin [9], it follows:

$$\int_{\Omega} p^{-1}\nabla\psi.\nabla u^h d\Omega - \int_{\Omega} \psi q k_0^2 u^h d\Omega - \int_{\Gamma} p^{-1}\psi\nabla u^h.\hat{\mathbf{n}} d\Gamma = 0 \tag{2}$$

where ψ is the test function.

Shape Function: RPIM Approximation

Meshless methods use a set of *randomly* spread nodes across the computation domain to build approximations of u^h. The nodes inside Ω are called *interior nodes*, and those located at Γ are called *boundary nodes*. In the approximation of the shape function using RPIM with polynomial reproduction, according to Liu [10], u^h at a point $\mathbf{x}$ is expressed as:

$$u^h(\mathbf{x}) = \sum_{i=1}^{n} R_i(\mathbf{x})a_i + \sum_{j=1}^{m} P_j(\mathbf{x})b_j = \mathbf{R}^T(\mathbf{x})\mathbf{a} + \mathbf{P}^T(\mathbf{x})\mathbf{b} \tag{3}$$

where a_i is the coefficient of the radial base functions (RBFs) R_i, b_j is the coefficient of the monomial P_j in the polynomial base, n is the number of nodes in the support domain of $\mathbf{x}$, and m is the number of monomials in the polynomial base. The vectors $\mathbf{R}$ and $\mathbf{P}$ are assembled with the RBF and polynomial terms evaluated at the point $\mathbf{x}$, while the coefficient vectors $\mathbf{a}$ and $\mathbf{b}$ are determined by satisfying the interpolation of the shape function at the nodes of the support domain and imposing the constraint to assure a unique solution, as documented by Liu [10]. There follows:

$$\mathbf{b} = \mathbf{S}_b\mathbf{U}_s, \quad \mathbf{S}_b = [\mathbf{P}_m^T\mathbf{R}_Q^{-1}\mathbf{P}_m]^{-1}[\mathbf{R}_Q^{-1}\mathbf{P}_m]^T \tag{4}$$

$$\mathbf{a} = \mathbf{S}_a\mathbf{U}_s, \quad \mathbf{S}_a = \mathbf{R}_Q^{-1} - \mathbf{R}_Q^{-1}\mathbf{P}_m\mathbf{S}_b \tag{5}$$

where $\mathbf{R}_Q$ and $\mathbf{P}_m$ are the moment matrices associated with $\mathbf{R}(\mathbf{x})$ and $\mathbf{P}(\mathbf{x})$, respectively, evaluated at all support nodes. Amongst several options for the RBFs, as described by Liu [11], the Multiquadratics RBF was chosen for being the most robust.

Hence, the vectors $\mathbf{\Phi}$ and $\mathbf{U_s}$ compile all the shape functions and field variables in the support domain, respectively. Finally, the approximation is given by:

$$u^h(\mathbf{x}) = [\mathbf{R}^T(\mathbf{x})\mathbf{S}_a + \mathbf{P}^T(\mathbf{x})\mathbf{S}_b]\mathbf{U}_s = \mathbf{\Phi}(\mathbf{x})\mathbf{U}_s. \tag{6}$$

In summary, the shape functions and their directional derivatives are given by, respectively:

$$\mathbf{\Phi}(\mathbf{x}) = \mathbf{R}^T(\mathbf{x})\mathbf{S}_a + \mathbf{P}^T(\mathbf{x})\mathbf{S}_b \tag{7}$$

$$\hat{\mathbf{n}}.\nabla\mathbf{\Phi}(\mathbf{x}) = \frac{\partial\mathbf{\Phi}(\mathbf{x})}{\partial n} = \frac{\partial\mathbf{R}^T(\mathbf{x})}{\partial n}\mathbf{S}_a + \frac{\partial\mathbf{P}^T(\mathbf{x})}{\partial n}\mathbf{S}_b. \tag{8}$$

The MLPG Collocation Approach

At each node i (for both interior and boundary nodes), a shape function is associated, whose compact support Ω_i is a circle with radius R_c. The support domain used to build the shape function is a circle with radius R_s, sufficiently larger than R_c to assure that the numerical integration points are inside the interpolation region of the shape function. In addition to the shape function, another function, called the *test function*, is associated with the interior nodes only. This test function ψ_i acts in a specific region surrounding the node called the node's *test domain*. In this case, in order to simplify the formulation, the radius of the circular test domain was also chosen to be R_c.

To avoid the process of finding the intersection between the test domain Γ_i and the global boundary Γ, which may be a burdensome process depending on the geometry of Γ, the test domain radius is chosen in a manner that the test domain Γ_i is tangent to Γ.

Figure 1 shows a simplified scheme of this approach. The nodes inside the domain Ω and whose test domains do intersect the global boundary Γ, like the node j has, their test domain Γ_j is reduced to osculate Γ. Nodes at Γ, like the node k are treated by a collocation approach in the coupling stage.

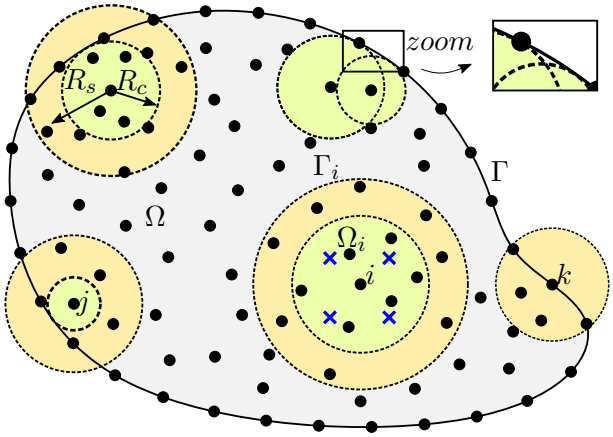

Figure 1. MLPG collocation scheme.

Amongst the several MLPG formulations in the literature, the one implemented was the same presented by Liu [11], where the test function is given by:

$$\psi(s) = \begin{cases} \frac{2}{3} - 4s^2 + 4s^3 & s < \frac{1}{2} \\ \frac{4}{3} - 4s + 4s^2 - \frac{4}{3}s^3 & \frac{1}{2} \leq s < 1 \\ 0 & s \geq 1 \end{cases} \tag{9}$$

where the definition was normalized using $s = |\mathbf{x} - \mathbf{x}_i|/R_c$, given that $\mathbf{x}$ is a point where the solution is approximated, $\mathbf{x_i}$ is the node in the center of the subdomain and R_c is its radius.

According to Nicomendes et al. [5], this MLPG colocation approach converges if the union of the subdomains Ω_i, for every internal node i, covers approximately all the computation domain Ω. Therefore, the following requirement must be satisfied:

$$\bigcup_{i \in \Omega} \Omega_i \approx \Omega. \tag{10}$$

Accordingly, considering the simplifications, the equation to be dealt with is:

$$\int_{\Omega_i} p^{-1}\nabla\psi\nabla u^h d\Omega - \int_{\Omega_i} \psi q k_0^2 u^h d\Omega = 0. \tag{11}$$

In a matrix form, the iteration between the global nodes i and j is given by K_{ij} is described by:

$$K_{ij} = \int_{\Omega_i} p^{-1}\nabla\psi_i.\nabla\phi_j d\Omega - \int_{\Omega_i} k_0^2 q\psi_i\phi_j d\Omega. \tag{12}$$

If the function ϕ_j associated with the global node j does not influence the subdomain Ω_i associated with the global node i, $K_{ij} = 0$.

2.2 External Region: Method of Moments

TMz Polarization

In the external region and for the TMz polarization, the equivalence principle is applied to establish the EFIE and MFIE in a 2-dimensional space, which according to Gibson [6] are, respectively:

$$[j\omega\mu(\mathcal{L}\mathbf{J}) + (\mathcal{K}\mathbf{M})]_{tan} + \frac{1}{2}\hat{\mathbf{n}}(\boldsymbol{\rho}) \times \mathbf{M}(\boldsymbol{\rho}) = \left[\mathbf{E}^i\right]_{tan} \tag{13}$$

$$[j\omega\epsilon(\mathcal{L}\mathbf{M}) + (\mathcal{K}\mathbf{J})]_{tan} - \frac{1}{2}\hat{\mathbf{n}}(\boldsymbol{\rho}) \times \mathbf{J}(\boldsymbol{\rho}) = \left[\mathbf{H}^i\right]_{tan} \tag{14}$$

where the operators $\mathcal{L}$ and $\mathcal{K}$ are:

$$(\mathcal{L}\mathbf{X})(\boldsymbol{\rho}) = \left[1 + \frac{1}{k^2}\nabla\nabla.\right] \int_V G(\boldsymbol{\rho}, \boldsymbol{\rho'})\mathbf{X}(\boldsymbol{\rho'})d\boldsymbol{\rho'} \tag{15}$$

$$(\mathcal{K}\mathbf{X})(\boldsymbol{\rho}) = \nabla \times \int_V G(\boldsymbol{\rho}, \boldsymbol{\rho'})\mathbf{X}(\boldsymbol{\rho'})d\boldsymbol{\rho'} \tag{16}$$

given that the free space 2-dimensional Green's function is:

$$G(\boldsymbol{\rho}, \boldsymbol{\rho'}) = \frac{-j}{4} H_0^{(2)}(k|\boldsymbol{\rho} - \boldsymbol{\rho'}|). \tag{17}$$

Noticing that $H_0^{(2)}$ is the Hankel function of 2$^{\text{nd}}$ kind and order 0, and E^i and H^i are the electric and magnetic incident fields, respectively. Moreover, $\mathbf{J}$ and $\mathbf{M}$ are the electric and magnetic equivalent current densities, respectively. Figure 2 shows the adopted vectorial system.

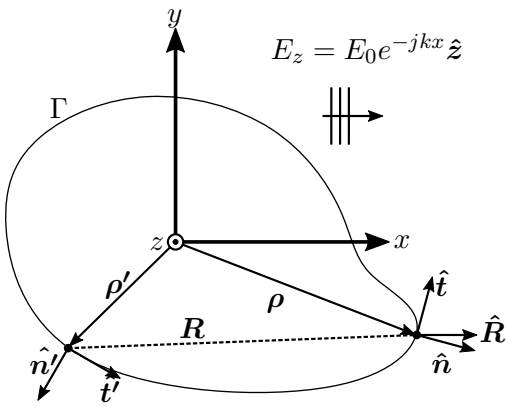

Figure 2. Vectorial system used for an arbitrary cylinder shape Γ.

After applying the known functions f^z and g^t, where the superscript relates to z-direction and tangent-direction to the boundary Γ, to represent the equivalent current densities and the test functions, implemented using triangular functions, the Eqs. (13) and (14) are represented in a linear matrix system:

$$\begin{bmatrix} L^{zz} & K^{zt} \\ -K^{tz} & \frac{\epsilon}{\mu}L^{tt} \end{bmatrix} \begin{bmatrix} J^z \\ M^t \end{bmatrix} = \begin{bmatrix} V^{E,TM} \\ V^{H,TM} \end{bmatrix} \tag{18}$$

where:

$$L^{zz} = \frac{\omega\mu}{4} \int_{\mathbf{f}_m^z} \mathbf{f}_m^z(\boldsymbol{\rho}) \cdot \int_{\mathbf{f}_n^z} \mathbf{f}_n^z(\boldsymbol{\rho'}) H_0^{(2)}(k|\boldsymbol{\rho} - \boldsymbol{\rho'}|) d\boldsymbol{\rho'} d\boldsymbol{\rho} \tag{19}$$

$$K^{zt} = \frac{1}{2} \int_{\mathbf{f}_m^z = \mathbf{g}_n^t} \mathbf{f}_m^z(\boldsymbol{\rho}) \cdot \left[\hat{\mathbf{n}} \times \mathbf{g}_n^t(\boldsymbol{\rho})\right] d\boldsymbol{\rho} - \frac{jk}{4} \int_{\mathbf{f}_m^z} \mathbf{f}_m^z(\boldsymbol{\rho}) \cdot \int_{\mathbf{g}_n^t} \mathbf{g}_n^t(\boldsymbol{\rho'}) \times \hat{\mathbf{R}}(\boldsymbol{\rho}, \boldsymbol{\rho'}) H_1^{(2)}(k|\boldsymbol{\rho} - \boldsymbol{\rho'}|) d\boldsymbol{\rho'} d\boldsymbol{\rho} \tag{20}$$

$$K^{tz} = \frac{1}{2} \int_{\mathbf{g}_m^t = \mathbf{f}_n^z} \mathbf{g}_m^t(\boldsymbol{\rho}) \cdot \left[\hat{\mathbf{n}} \times \mathbf{f}_n^z(\boldsymbol{\rho})\right] d\boldsymbol{\rho} - \frac{jk}{4} \int_{\mathbf{g}_m^t} \mathbf{g}_m^t(\boldsymbol{\rho}) \cdot \int_{\mathbf{f}_n^z} \mathbf{f}_n^z(\boldsymbol{\rho'}) \times \hat{\mathbf{R}}(\boldsymbol{\rho}, \boldsymbol{\rho'}) H_1^{(2)}(k|\boldsymbol{\rho} - \boldsymbol{\rho'}|) d\boldsymbol{\rho'} d\boldsymbol{\rho} \tag{21}$$

$$L^{tt} = \frac{\omega\mu}{4} \int_{\mathbf{g}_m^t} \mathbf{g}_m^t(\boldsymbol{\rho}) \cdot \int_{\mathbf{g}_n^t} \mathbf{g}_n^t(\boldsymbol{\rho'}) H_0^{(2)}(k|\boldsymbol{\rho} - \boldsymbol{\rho'}|) d\boldsymbol{\rho'} d\boldsymbol{\rho} - \frac{1}{4\omega\epsilon} \int_{\mathbf{g}_m^t} \nabla \cdot \mathbf{g}_m^t(\boldsymbol{\rho}) \cdot \int_{\mathbf{g}_n^t} \nabla' \cdot \mathbf{g}_n^t(\boldsymbol{\rho'}) H_0^{(2)}(k|\boldsymbol{\rho} - \boldsymbol{\rho'}|) d\boldsymbol{\rho'} d\boldsymbol{\rho} \tag{22}$$

$$V^{E,TM} = \int_{\mathbf{f}_m^z} \mathbf{f}_m^z(\boldsymbol{\rho}) \cdot \mathbf{E}^i(\boldsymbol{\rho}) d\boldsymbol{\rho} \tag{23}$$

$$V^{H,TM} = \int_{\mathbf{g}_m^t} \mathbf{g}_m^t(\boldsymbol{\rho}) \cdot \mathbf{H}^i(\boldsymbol{\rho}) d\boldsymbol{\rho}. \tag{24}$$

Although the outer region is vacuum, this general formulation considers an arbitrary homogeneous medium where k is its wavenumber, ϵ is its electric permittivity and μ is its magnetic permeability.

TEz Polarization

The operators of the EFIE for the TEz polarization are the dual of those of the MFIE for the TMz polarization, where the electric and magnetic currents are exchanged with each other. Likewise, the operators of the MFIE for the TEz polarization are the dual of those of the EFIE for the TMz polarization, with electric and magnetic currents are exchanged with each other. Thus, leading to the matricial system:

$$\begin{bmatrix} L^{tt} & K^{tz} \\ -K^{zt} & \frac{\epsilon}{\mu}L^{zz} \end{bmatrix} \begin{bmatrix} J^t \\ M^z \end{bmatrix} = \begin{bmatrix} V^{E,TE} \\ V^{H,TE} \end{bmatrix} \tag{25}$$

where:

$$V^{E,TE} = \int_{\mathbf{g}_m^t} \mathbf{g}_m^t(\boldsymbol{\rho}) \cdot \mathbf{E}^i(\boldsymbol{\rho}) d\boldsymbol{\rho} \tag{26}$$

$$V^{H,TE} = \int_{\mathbf{f}_m^z} \mathbf{f}_m^z(\boldsymbol{\rho}) \cdot \mathbf{H}^i(\boldsymbol{\rho}) d\boldsymbol{\rho}. \tag{27}$$

Scattering Field Calculation

In the outer region, once $\mathbf{J}$ and $\mathbf{M}$ are solved, the scattering field can be calculated by Eq. (28) for the TMz polarization and Eq. (29) for the TEz polarization. The total field is the sum of the scattering and the incident field.

$$E_z^s(\boldsymbol{\rho}) = -\frac{k^2}{4\omega\epsilon} \int_\Gamma \mathbf{J}(\boldsymbol{\rho'}) H_0^{(2)}(k|\boldsymbol{\rho} - \boldsymbol{\rho'}|) d\boldsymbol{\rho'} - j\frac{k}{4} \int_\Gamma (\boldsymbol{\rho} - \boldsymbol{\rho'}) \times \mathbf{M}(\boldsymbol{\rho'}) \frac{H_1^{(2)}(k|\boldsymbol{\rho} - \boldsymbol{\rho'}|)}{|\boldsymbol{\rho} - \boldsymbol{\rho'}|} d\boldsymbol{\rho'} \tag{28}$$

$$H_z^s(\boldsymbol{\rho}) = +\frac{k^2}{4\omega\epsilon} \int_\Gamma \mathbf{M}(\boldsymbol{\rho'}) H_0^{(2)}(k|\boldsymbol{\rho} - \boldsymbol{\rho'}|) d\boldsymbol{\rho'} - j\frac{k}{4} \int_\Gamma (\boldsymbol{\rho} - \boldsymbol{\rho'}) \times \mathbf{J}(\boldsymbol{\rho'}) \frac{H_1^{(2)}(k|\boldsymbol{\rho} - \boldsymbol{\rho'}|)}{|\boldsymbol{\rho} - \boldsymbol{\rho'}|} d\boldsymbol{\rho'}. \tag{29}$$

2.3 The Coupling Interface

As both methods possess functions with the Kronecker's delta property, in order to couple the numerical methods in the different regions, it is only required that the tangential components of the electromagnetic field are continuous at the interface. According to Harrington [12], that is achievable forcing the following equations:

$$\mathbf{J} = \hat{\mathbf{n}} \times \mathbf{H} \tag{30}$$

$$\mathbf{E} = \hat{\mathbf{n}} \times \mathbf{M}. \tag{31}$$

TMz Polarization

For the TMz polarization, using the collocation method, Equation (30) is forced directly into the matricial system of the intern problem. There follows:

$$K_{ij} = \nabla\phi_j(\mathbf{x_i}).\hat{\mathbf{n}} \tag{32}$$

$$J_{ij}^K = \begin{cases} 0 & \forall i \in \Omega \\ -j\omega\mu\phi_j(\mathbf{x_i}) & \forall i \in \Gamma \end{cases} \tag{33}$$

where J_z is only defined over Γ. The columns of J_{ij}^K associated to the j nodes that are in Ω are eliminated. The remainder Eq. (31) is dealt in the same manner, leading to:

$$\begin{cases} U_{ij} = +\phi_j(\mathbf{x_i}) & \forall i \in \Gamma \\ M_{ij}^U = -\phi_j(\mathbf{x_i}) & \forall i \in \Gamma. \end{cases} \tag{34}$$

TEz Polarization

For the TEz polarization, using the collocation method, Equation (31) is forced directly into the matricial system of the intern problem. There follows:

$$K_{ij} = \nabla\phi_j(\mathbf{x_i}).\hat{\mathbf{n}} \tag{35}$$

$$M_{ij}^K = \begin{cases} 0 & \forall i \in \Omega \\ j\omega\mu\phi_j(\mathbf{x_i}) & \forall i \in \Gamma \end{cases} \tag{36}$$

where M_z is only defined over Γ, and the columns of M_{ij}^K associated to the j nodes that are in Ω are eliminated. The remainder Eq. (31) is dealt in the same manner, leading to:

$$\begin{cases} U_{ij} = +\phi_j(\mathbf{x_i}) & \forall i \in \Gamma \\ J_{ij}^U = +\phi_j(\mathbf{x_i}) & \forall i \in \Gamma. \end{cases} \tag{37}$$

2.4 The Complete System

Therefore, the complete matricial system is given by:

$$\begin{bmatrix} K_{(n\times n)} & J_{(n\times m)}^K & M_{K\,(n\times m)} \\ U_{(m\times n)} & J_{(M\times m)}^U & M_{(m\times m)}^U \\ 0_{(m\times n)} & Z_{(m\times m)}^J & Z_{(m\times m)}^M \end{bmatrix} \begin{bmatrix} u^h \\ J \\ M \end{bmatrix} = \begin{bmatrix} 0_{(n\times 1)} \\ 0_{(m\times 1)} \\ Z_{(m\times 1)}^V \end{bmatrix} \tag{38}$$

where n is the sum of interior and boundary nodes and m is the number of boundary nodes. For the TMz polarization, all elements of M^k and J^U are zero, while for the TEz polarization, all elements of J^k and M^U are zero. The matrices Z^J, Z^M and Z^V are built linearly combining both EFIE and MFIE equations, resulting in:

$$TM: \begin{cases} Z^J &= \alpha L^{zz} - (1-\alpha)\eta K^{tz} \\ Z^M &= \alpha K^{zt} + (1-\alpha)\eta^{-1} L^{tt} \\ Z^V &= \alpha V^{E,TM} + (1-\alpha)\eta V^{H,TM} \end{cases} \quad TE: \begin{cases} Z^J &= \alpha L^{tt} - (1-\alpha)\eta K^{zt} \\ Z^M &= \alpha K^{tz} + (1-\alpha)\eta^{-1} L^{zz} \\ Z^V &= \alpha V^{E,TE} + (1-\alpha)\eta V^{H,TE} \end{cases} \tag{39}$$

where α equals 0.5 corresponds to a combined field integral equation (CFIE), leading to smaller errors and more robustness, as researched by Resende et al. [7].

3 Results

In order to evaluate the MLPG/MoM formulation, a canonical problem was analyzed for both TMz and TEz polarizations: the scattering of a plane wave by a dielectric circular cylinder. The scatterer cylinder was placed with its center at the origin of the coordinate system. The outside medium is free space. The schematics of the problem is represented by the figure below for the TMz polarization.

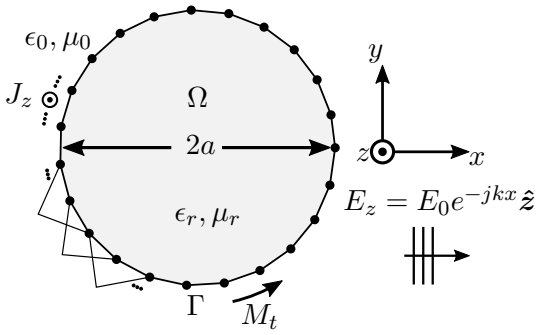

Figure 3. TMz polarization: scattering of a plane wave by a dielectric circular cylinder.

3.1 Homogeneous Case

This problem addresses the scattering by a dielectric circular cylinder with a homogeneous medium. The incident field is $E_z^i = e^{-jk_0 x}$ for the TMz polarization, and $H_z^i = e^{-jk_0 x}$ for the TEz polarization. The nodes were uniformly spread throughout the computational domain. The parameters are summarized in Table 1.

Table 1. Parameters used in the homogeneous simulation case

Properties	Value
Relative Dielectric Permittivity	3-0.1j
Cylinder Radius	0.5 λ_0
Total Number of Nodes	1045
Boundary Nodes (MoM)	109

TM Polarization

For the TMz polarization, Figures 4 and 5 show the results of the equivalent electric and magnetic current densities at the contour of the dielectric cylinder, respectively, while Fig. 6 shows the electric field at a line in the x-direction passing through the center of the cylinder.

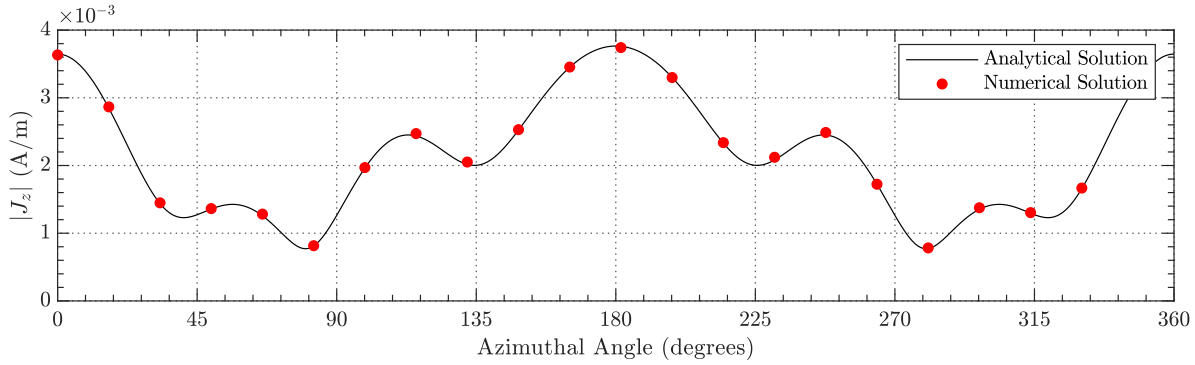

Figure 4. TMz polarization: amplitude of the equivalent electric current density.

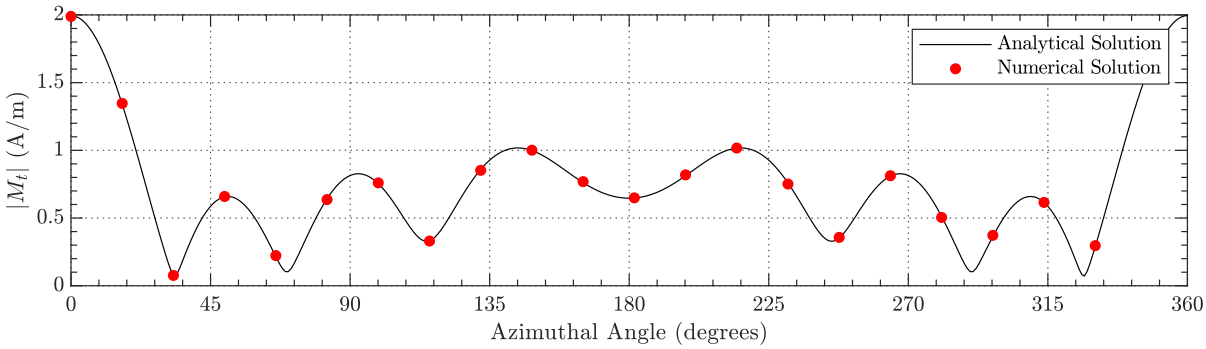

Figure 5. TMz polarization: amplitude of the equivalent magnetic current density.

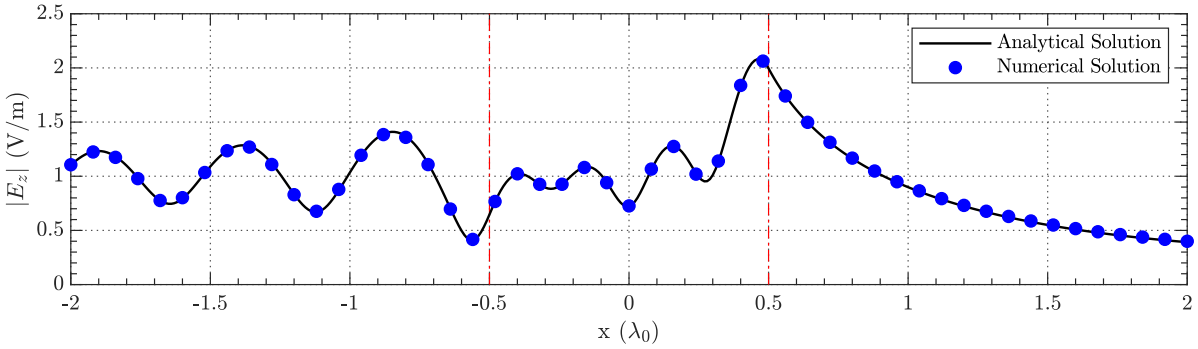

Figure 6. TMz polarization: amplitude of the electric field at $y = 0$.

The numerical results obtained show a good agreement with the analytical solutions. Figure 6 shows that the electric field and its first derivative are continuous throughout the entire space, which was already known since the magnetic permeability is continuous at the interface.

TE Polarization

For the TEz polarization, Figures 7 and 8 show the results of the equivalent electric and magnetic current densities at the contour of the dielectric cylinder, respectively, while Fig. 9 shows the electric field at a line in the x-direction passing through the center of the cylinder.

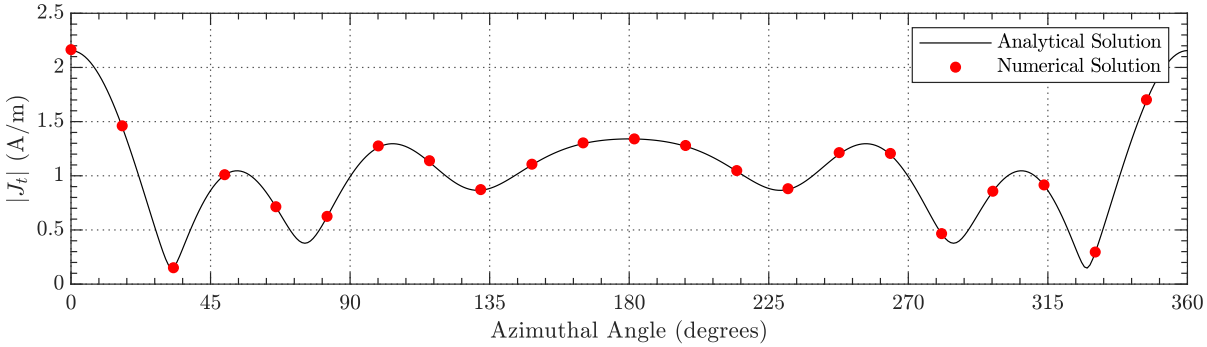

Figure 7. TEz polarization: Amplitude of the equivalent electric current density.

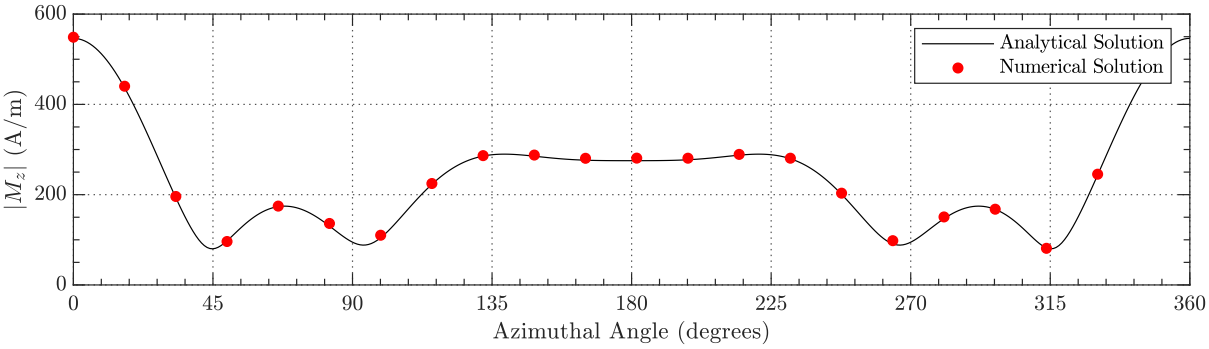

Figure 8. TEz polarization: amplitude of the equivalent magnetic current density.

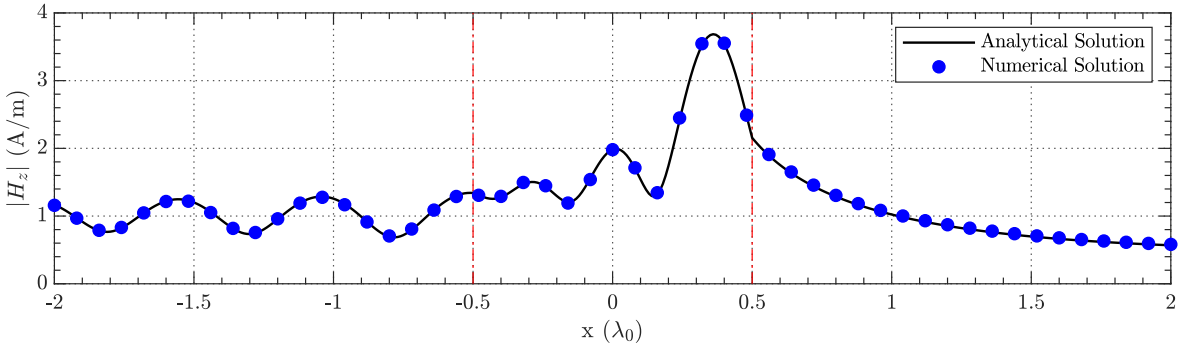

Figure 9. TEz polarization: amplitude of the magnetic field at $y = 0$.

The numerical results obtained show a good agreement with the analytical solutions. Unlike the TMz polarization, Figure 9 shows that the magnetic field is continuous throughout the entire space; however, its first derivative is discontinuous at the interface as a result of the electric permittivity discontinuity. Since the MLPG method uses continuous shape functions with continuous first derivatives, handling discontinuities using a pure meshless method demands a complex solution. This process is naturally handled by the hybrid MLPG-MoM approach.

Error Convergence

In order to determine the performance of the MLPG-MoM hybrid method, as the scattering of a plane wave by a circular cylinder has an analytical modal solution, the relative error was calculated for the electromagnetic field and the equivalent current densities. Figure 10 shows the error convergence analysis considering the discretization length h as the maximum internodal distance.

The relative error is calculated by the ratio of the difference between the solutions to the L^2 norm of the exact solution. It follows that:

$$L^2(X) = \frac{\sqrt{\int_{\nu_0} |X^{Numerical} - X^{Exact}|^2 \, d\nu}}{\sqrt{\int_{\nu_0} |X^{Exact}|^2 \, d\nu}} \tag{40}$$

where ν is Ω for the electromagnetic field and Γ for the equivalent current densities.

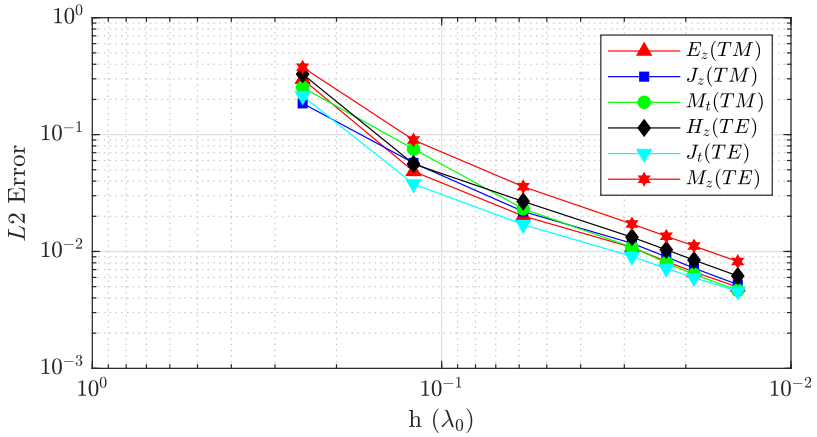

Figure 10. L2 norm error for the hybrid MLPG-MoM method.

This graph shows that all of the solution variables have comparable convergence rate, regardless of polarization. Since the exterior electromagnetic field is calculated based on the equivalent current densities, it also converges with the same convergence rate.

3.2 Inhomogenous Case

An advantage of the MLPG method is that it can easily handle inhomogeneous mediums. To address this class of problems, a 2-dimensional circular cylindric Lüneberg Lens was analyzed. This is a well-known lens that converges the energy of a plane wave at a single line, as seen in Fig. 11.

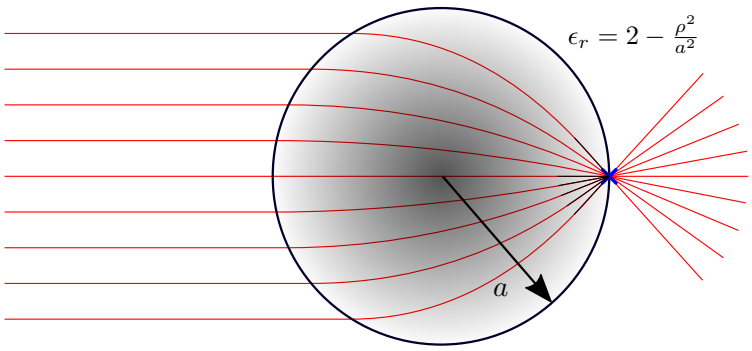

Figure 11. Qualitative diagram of a Lüneburg lens (where ρ is the radial axis considering the center of the cylinder at the origin of the polar coordinate system and the outside medium is vacuum).

The incident field is $E_z^i = e^{-jk_0x}$ for the TMz polarization and $H_z^i = e^{-jk_0x}$ for the TEz polarization. The nodes were uniformly spread throughout the computational domain. The parameters are summarized in Table 2.

Table 2. Parameters used in the inhomogeneous simulation case

Properties	Value
Cylinder Radius	2 λ_0
Total Number of Nodes	2512
Boundary Nodes (MoM)	172
Number of Elements (FEM)	69058
Number of Nodes (FEM)	34859

As an analytical solution does not exist for this problem, the numerical solution was compared to a well-refined FEM solution. The FEM computational domain used had a radius of $3\lambda_0$ plus a $0.5\lambda_0$ PML section. It was implemented using first-order elements with a locally-conformal PML formulation, as described by Ozgun et al. [13].

Figures 12 and 13 show the numerical solution compared to the FEM solution for both TM and TE polarizations, respectively.

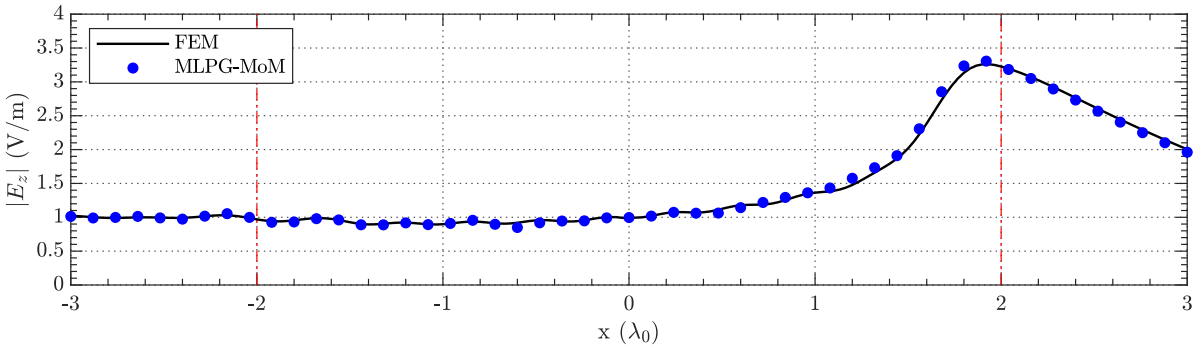

Figure 12. TM polarization: amplitude of the electric field at $y = 0$.

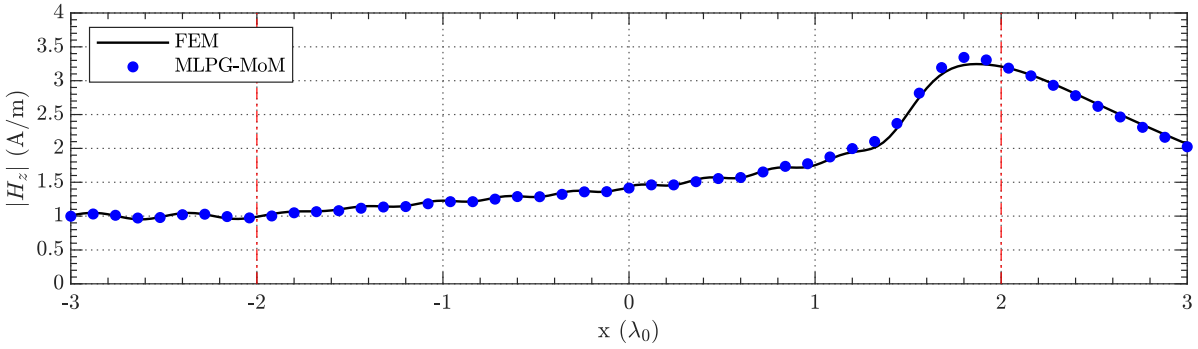

Figure 13. TE polarization: amplitude of the magnetic field at $y = 0$.

The numerical results obtained show a good agreement with the well-refined FEM solutions. For the TMz and TEz polarizations, there are no discontinuities given that the electric permissivity is continuous throughout all the space. Figure 14 shows the numerical solution in a $64\lambda_0^2$ area around the cylinder. The results agree with the expected qualitative behavior of a Luneberg lens.

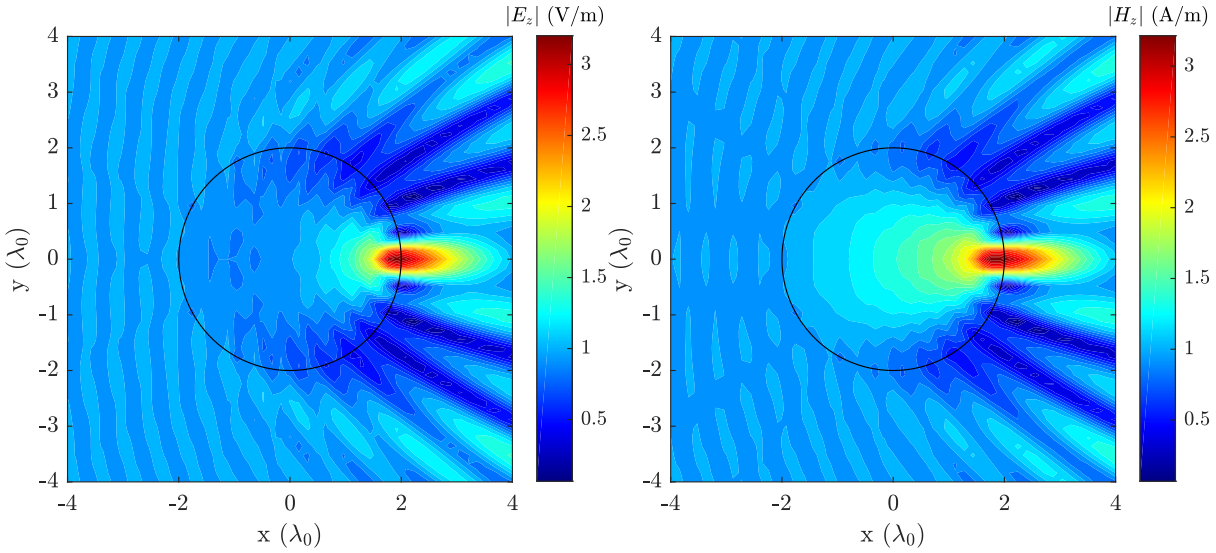

(a) TMz Polarization (b) TEz Polarization

Figure 14. Amplitude of the electric and magnetic fields.

4 Conclusions

This work proposed an alternative meshless formulation to handle scattering problems with unbounded domains. It combines the best properties of both methods. A bounded region is handled by a meshless method which is capable of modeling well complex geometries and inhomogeneous materials, whereas the outer free-space region is taken care by the method of moments which is efficient and easily applied to unbounded homogeneous mediums.

The hybrid MLPG-MoM proposed combines a meshless method, which does not require a mesh structure, and MoM, with equivalent current densities to be determined only at the scatter's surface allowing the calculation of the field in the entire space. In addition to the reduction of the computational domain, the meshless method can handle objects with complex geometries and continuous electric permissivity or magnetic permeability profiles. Moreover, unlike the pure meshless, this hybrid implementation can naturally deal with discontinuities at the interface.

For both TMz and TEz polarizations, the effectiveness and accuracy of the presented hybrid formulation were verified by analyzing the scattering of a plane wave by a homogeneous, and by an inhomogeneous dielectric cylinder. In the homogeneous case, the results were compared to the analytical solution of the problem. In the inhomogeneous case, the Luneberg lens problem was analyzed, which does not have an analytical solution; therefore the results were compared to a well-refined FEM solution, given that it is a well consolidated numerical method. For both study cases, the numerical results obtained showed a good agreement compared to the reference solutions.

The convergence rates for both polarizations were nearly the same, which was expected since the problems are dual, and only the TMz or TEz implementation is required for a dielectric cylinder. Since the outer field is calculated based on the equivalent current densities, it also led to comparable accuracy and similar convergence rate of the inner field.

Acknowledgements

This work was partially supported by CAPES/PROCAD (068419/14-01), CNPq and FAPEMIG.

References

[1] Liu, M. & Liu, G., 2010. Smoothed particle hydrodynamics (sph): an overview and recent developments. *Archives of computational methods in engineering*, vol. 17, n. 1, pp. 25–76.

[2] Lu, Y., Belytschko, T., & Gu, L., 1994. A new implementation of the element free galerkin method. *Computer methods in applied mechanics and engineering*, vol. 113, n. 3-4, pp. 397–414.

[3] Atluri, S. N. & Zhu, T., 1998. A new meshless local petrov-galerkin (mlpg) approach in computational mechanics. *Computational mechanics*, vol. 22, n. 2, pp. 117–127.

[4] Resende, U. C., Coppoli, E. H. R., & Afonso, M. M., 2015a. A meshless approach using efg interpolating moving least-squares method in 2-d electromagnetic scattering analysis. *IEEE Transactions on Magnetics*, vol. 51, n. 3, pp. 1–4.

[5] Nicomedes, W. L., Mesquita, R. C., & Moreira, F. J. S., 2012. The meshless local petrov–galerkin method in two-dimensional electromagnetic wave analysis. *IEEE Transactions on Antennas and Propagation*, vol. 60, n. 4, pp. 1957–1968.

[6] Gibson, W. C., 2007. *The method of moments in electromagnetics*. Chapman and Hall/CRC.

[7] Resende, U. C., Rosa, C., Avidago, A. G., Afonso, M., & Moreira, F. J. S., 2015b. A new meshless-mom hybrid method applied to the analisys of 2d electromagnetic scattering. In *ISEF20 15*. Valence.

[8] Peterson, A. F., Ray, S. L., Mittra, R., & IEEE, 1998. *Computational methods for electromagnetics*, volume 2. IEEE press New York.

[9] Jin, J.-M., 2015. *The finite element method in electromagnetics*. John Wiley & Sons.

[10] Liu, G.-R., 2009. *Meshfree methods: moving beyond the finite element method*. CRC press.

[11] Liu, G.-R. & Gu, Y.-T., 2005. *An introduction to meshfree methods and their programming*. Springer Science & Business Media.

[12] Harrington, R. F., 1961. *Time-harmonic electromagnetic fields*. McGraw-Hill.

[13] Özgün, Ö. & Kuzuoğlu, M., 2018. *MATLAB-based Finite Element Programming in Electromagnetic Modeling*. CRC Press.